AGU PUBLICATIONS

Geophysical Research Letters

RESEARCH LETTER
10.1002/2015GL065841

Key Points:
- Model-proxy comparisons in terminal lake basins contextualize past and present hydroclimates
- Climate conditions require decadal persistence to elicit complete lake-level oscillations
- The current CA-NV drought exceeds past droughts in mean severity but not duration

Supporting Information:
- Supporting Information S1
- Figure S1
- Figure S2

Correspondence to:
B. J. Hatchett,
benjamin.hatchett@gmail.com

Citation:
Hatchett, B. J., D. P. Boyle, A. E. Putnam, and S. D. Bassett (2015), Placing the 2012–2015 California-Nevada drought into a paleoclimatic context: Insights from Walker Lake, California-Nevada, USA, *Geophys. Res. Lett.*, *42*, 8632–8640, doi:10.1002/2015GL065841.

Received 19 AUG 2015
Accepted 16 SEP 2015
Published online 28 OCT 2015

Placing the 2012–2015 California-Nevada drought into a paleoclimatic context: Insights from Walker Lake, California-Nevada, USA

Benjamin J. Hatchett[1], Douglas P. Boyle[1], Aaron E. Putnam[2,3], and Scott D. Bassett[1]

[1]Department of Geography, University of Nevada, Reno, Reno, Nevada, USA, [2]School of Earth and Climate Sciences and Climate Change Institute, University of Maine, Orono, Maine, USA, [3]Lamont-Doherty Earth Observatory, Columbia University, New York City, New York, USA

Abstract Assessing regional hydrologic responses to past climate changes can offer a guide for how water resources might respond to ongoing and future climate change. Here we employed a coupled water balance and lake evaporation model to examine Walker Lake behaviors during the Medieval Climate Anomaly (MCA), a time of documented hydroclimatic extremes. Together, a ^{14}C-based shoreline elevation chronology, submerged subfossil tree stumps in the West Walker River, and regional paleoproxy evidence indicate a ~50 year pluvial episode that bridged two 140+ year droughts. We developed estimates of MCA climates to examine the transient lake behavior and evaluate watershed responses to climate change. Our findings suggest the importance of decadal climate persistence to elicit large lake-level fluctuations. We also simulated the current 2012–2015 California-Nevada drought and found that the current drought exceeds MCA droughts in mean severity but not duration.

1. Introduction

Continued population and economic growth in semiarid regions increase pressure on limited existing natural resources [*Montenegro and Ragab,* 2012]. Under scenarios of future climate warming, water scarcity in these regions will likely increase [*Seager et al.,* 2007; *Broecker*, 2010; *Broecker and Putnam,* 2013; *Dai,* 2013]. Despite uncertainty in projected precipitation changes in complex terrain [*Mearns et al.,* 2012], higher ambient air temperatures produced by background warming alone negatively forces the water balance [*Dai et al.,* 2004; *Cayan et al.,* 2010], thereby enhancing drought risk [*Cook et al.,* 2015; *Diffenbaugh et al.,* 2015]. Understanding patterns and possible causes of past hydroclimatic changes provides insight into present and future drought risk and helps to inform policymakers, resource managers, and the general public about potential socioeconomic consequences and impacts on ecological wealth in dryland regions [*Stakhiv,* 2011].

Here we ask the question as to whether the hydroclimate conditions occurring during the water years 2012–2015 (hereafter current) drought in California-Nevada are within the range of natural variability documented by paleoproxy indicators and thus aid disentanglement of the relative roles of natural versus anthropogenic forcing factors as causative agents [e.g., *Seager et al.,* 2015]. Starting in late 2011, persistent sea surface temperature anomalies forced midtropospheric blocking in the eastern North Pacific Ocean, resulting in a poleward deflection of storm tracks and reduced moisture flux into the California-Nevada region [*Swain et al.,* 2014; *Wang et al.,* 2014; *Wang and Schubert,* 2014; *Seager et al.,* 2015]. In comparing historical droughts that occurred between 1912 and 2012, *Shukla et al.* [2015] demonstrated that anomalously warm temperatures have amplified the severity of the current drought. Impacts include altered nutrient cycling in aquatic ecosystems [*Schladow,* 2014], increased rates of Sierra Nevada uplift [*Borsa et al.,* 2014], and reductions in California state and federal water project deliveries for water year 2015 [*California Department of Water Resources,* 2015; *U.S. Bureau of Reclamation,* 2015]. Economic losses in California linked to drought conditions were estimated at $2.2 billion for 2014 [*Howitt et al.,* 2014].

By employing model simulations of past and current drought in the California-Nevada region, we attempt to place the current drought into a paleoclimatic context. We use a water balance model together with a lake evaporation model to simulate lake level and streamflow responses to changes in precipitation and temperature in the Walker Lake Basin (WLB; 38.5°N, 119°W; Figure 1a). Walker Lake is a terminal lake whose surface area and elevation are functions of outgoing evaporative losses and inputs from direct precipitation and watershed-derived runoff. As

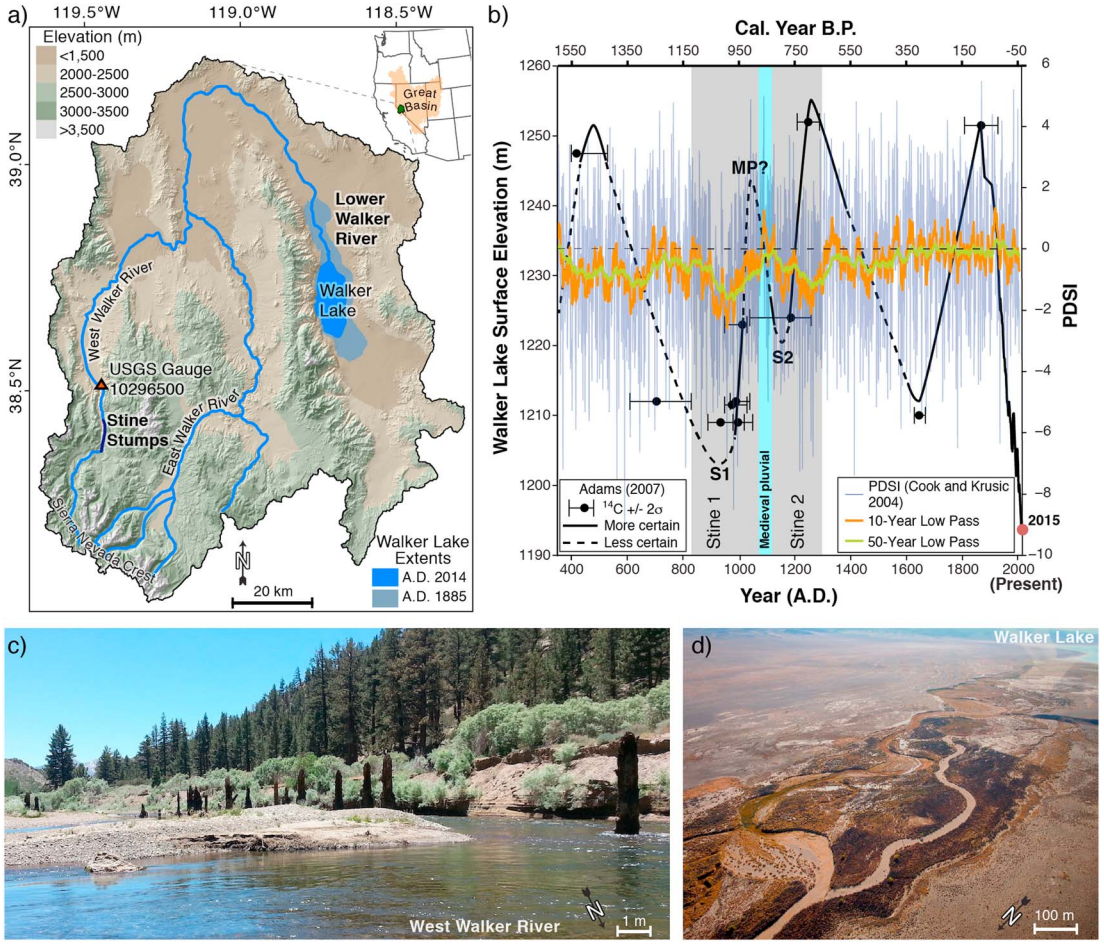

Figure 1. (a) Map of the Walker Lake Basin showing the West Walker River (WWR), the Lower Walker River, the historic (light blue fill) and 2014 (dark blue fill) extents of Walker Lake, and the location of the submerged stumps (dark blue line). (b) Paleoproxy data used in the study including the Walker Lake level reconstruction of *Adams* [2007] (thick and dashed black lines, interpreted Stine lowstands and Medieval Pluvial highstand indicated by S1, S2, and MP, respectively), the Stine droughts where tree growth occurred in the WWR, and the raw (blue) and low-pass-filtered (10 and 50 year, orange and green, respectively) North American Drought Atlas Palmer Drought Severity Index values [*Cook and Krusic,* 2004] for the interpolated grid point of the Walker Lake Basin centroid. (c) View of the WWR and submerged tree stumps. (d) Aerial view of the Lower Walker River's incision into lake deposits that allowed *Adams* [2007] to produce the lake level reconstruction curve in Figure 1b.

recorders of regional water balance, terminal lake levels provide metrics to assess regional climate change. Using the modeling framework mentioned above, we assessed the magnitude, duration, and transient behavior of water balance in Walker Lake and the WLB watershed for two cases: (1) The persistent droughts of the Medieval Climate Anomaly (MCA; circa A.D. 850–1300) [*Stine,* 1994; *Mann et al.,* 2009] and (2) the current drought. During MCA time, two 140+ year droughts were separated by a ~50 year wet episode in the California-Nevada region. *Adams* [2007] interpreted Walker Lake to have undergone an oscillation from lowstand to highstand to lowstand (relative to late Holocene levels; Figure 1b). We address the following questions: (1) under what climatic conditions could *Adams'* [2007] hypothesized MCA oscillation be feasible? And (2) can we use paleoproxy evidence to estimate and compare MCA droughts with the current drought in the WLB?

2. Geological Constraints on Medieval Hydroclimate

Stine [1994] identified and dated two sets of submerged subfossil stumps of *Pinus jeffreyi* in the West Walker River (WWR; 38.4°N, 119.45°W; Figures 1a–1c). This particular *Pinus* species cannot survive basal inundation for more than several weeks [*Stine*, 1994]. The chronology of *Stine* [1994] indicates that the trees were growing during two low-water phases of the MCA when WWR streamflow was sufficiently low to allow tree establishment and persistence. *Cook et al.* [2010] informally called these low-water phases the "Stine droughts" (S1; A.D. 832–1074, and S2; A.D. 1122–1299, standard deviation of 50 years). The dates that these

trees were killed represent terminations of these MCA droughts, i.e., when the level of the WWR rose and submerged their roots. The Stine droughts are separated by a transition to a wetter climate (informally called the Medieval Pluvial or MP) that lasted approximately 50 years (circa 1075–1125 A.D.; Figure 1b).

In addition, *Adams* [2007] developed a stratigraphic record of Late Holocene lake level fluctuations (Figure 1b). The stratigraphic framework was based on sedimentary interpretations of deltaic sediments along the Lower Walker River (Figures 1a and 1d) and supported by ^{14}C data. Corroborative regional evidence for the Stine droughts and the MP is provided by the tree ring-based North American Drought Atlas (Figure 1b) [*Cook and Krusic*, 2004; *Cook et al.,* 2004, 2010]. Other regional paleoproxy evidence also supports the S1-MP-S2 sequence. This evidence includes submerged trees in Mono and Tenaya Lakes [*Stine*, 1990, 1994], low levels of Pyramid Lake [*Benson et al.,* 2002], and two periods of lowered freshwater input into the San Francisco Bay Delta separated by a brief departure toward increased freshwater input [*Malamud-Roam and Ingram*, 2004]. Although not in perfect agreement, these paleoproxy data are consistent with *Adams'* [2007] S1-MP-S2 sequence.

3. Methods

We used a simple, calibrated water balance model (WBM) to estimate the S1-MP-S2 lake oscillation. WBMs have been used extensively for climate applications in the western United States [e.g., *McCabe and Wolock,* 2007, 2014; *Gray and McCabe,* 2010; *Saito et al.,* 2014]. The WBM used in the present study simulates the key components of the hydrologic cycle and their seasonal distribution. These components include the partitioning of precipitation into frozen and liquid components, snowpack accumulation and melting, soil water storage, evapotranspiration, and runoff (see *McCabe and Markstrom* [2007] for details). The WBM utilizes the algorithms presented by *McCabe and Markstrom* [2007]. It is distributed over the watershed at 800 m grid resolution to create a total of 14,756 model units. Each model unit is individually treated by the WBM algorithms at monthly time steps using inputs of monthly precipitation and maximum and minimum temperature from the Parameter-elevation Regressions on Independent Slopes Model (PRISM) [*Daly et al.,* 1994]. In addition to the WBM, the present study also employs a lake evaporation model (LEM). The LEM estimates the lake volume change based upon the inflow provided by the total monthly runoff produced by the WBM, direct precipitation on the lake, and the estimated evaporative losses from the lake. Losses are estimated with the Priestley-Taylor equation [*Priestley and Taylor,* 1972] as functions of temperature and lake surface area. The WBM and LEM are run with a monthly climatology until the annual change in lake elevation is less than 0.05%, at which point a steady state solution is achieved. Schematics of the WBM and LEM are provided in Figure S1 in the supporting information.

We performed model simulations aimed at dated geomorphic targets (paleoshorelines at different elevations) in order to estimate MCA hydroclimates for comparison to the current drought. We selected the following interpreted paleoshorelines from *Adams* [2007]: (1) interpreted lowstands of the S1 and S2 droughts at 1203 m and 1221 m, respectively, to characterize the Stine MCA droughts and (2) the interpreted MP highstand of 1245 m.

Our baseline model input climatology (*baseline*; simulations are italicized) used monthly PRISM averages from A.D. 1971 to 2000. It should be noted that the baseline climate is a relatively wet period (Figure S2). Initially, we held the temperature constant throughout the year; however, in two simulations, the temperature constraint was relaxed. Precipitation changes were applied equally to all model units between October and April as a multiplier of the baseline monthly precipitation climatology values (referred to as ΔP). Upon determining the precipitation multipliers which, when applied to the baseline climate, produced steady state lake surface elevations for the S1, S2, and MP interpreted shoreline elevations, we performed dynamic simulations of the lake-watershed system. The model was equilibrated to the *S1* climate using 10 years of the estimated steady state *S1* climate starting at the S1 lowstand (1203 m). We then changed the climate to the *MP* climate for 50 years. The climate was again shifted to the estimated steady state *S2* climatology for 200 years. For this simulation, the additional constraint requiring the lake to fall to at least 1224 m during the S2 interval is provided by a ^{14}C date (Figure 1b).

We provide six additional simulations. (1) The baseline climate applied during the MP. (2) The PRISM-estimated transient climate during the twentieth century pluvial (*TCP*; A.D. 1905–1917), which was an unusually wet episode in the past millennium in the southwestern United States [*Woodhouse et al.,* 2005; *Cook et al.,* 2011].

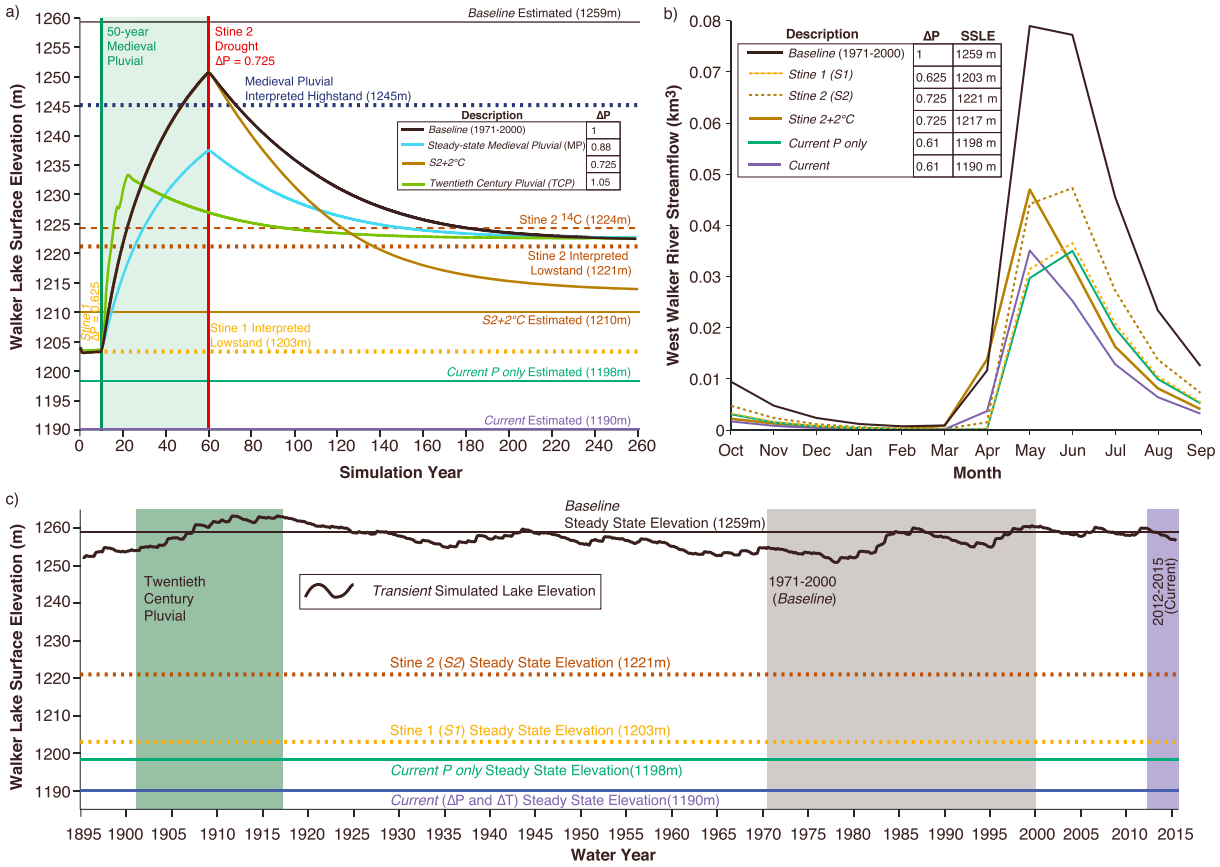

Figure 2. (a) Transient lake level simulation results under the scenarios of increased precipitation during the Medieval Pluvial and Stine 2 drought scenarios (thick colored lines). The thin colored lines indicate the model-estimated baseline and current drought steady state lake elevations. The dotted (dashed) lines indicate interpreted (dated) shoreline elevations. (b) Simulated West Walker River streamflow for the *baseline* (black line), *S1* (dashed yellow line), *S2* (dashed brown line), *S2* + 2°C (brown line), water years 2012–2015 precipitation only simulation (*Current P only*; green line) and precipitation and temperature simulation (*Current*; purple line). (c) *Transient* simulation of Walker Lake spanning water years 1895–2015 (ending June) initialized the late 1800s lake level of 1252 m. Key periods are highlighted with boxes and steady state lake elevations for various simulations are shown as dashed and thin lines.

(3) A simulation using the *S2* precipitation multiplier, but with the temperature constraint relaxed (*S2* + 2°C). We increased annual temperatures in this simulation by 2°C to demonstrate the effect of a warmer mean climate on the rate of lake level decline. (4) A simulation using only the PRISM-estimated precipitation from October to April of water years 2012–2015 (*Current P only*). The purpose is to compare the steady state lake level and streamflow under the current drought precipitation regime to the Stine drought estimated lake levels and streamflow. (5) A simulation using both the current drought's PRISM-estimated precipitation multipliers and temperature anomalies (*Current*). This simulation allows a comparison of how observed positive temperature anomalies exacerbate negative precipitation anomalies. (6) A transient lake simulation (*transient*) spanning water years 1895–2015 is performed with PRISM-estimated precipitation and temperature to demonstrate how interannual variability alone is insufficient to produce lake level changes on the order of those associated with MCA droughts and that decadal persistence of an average climate (inclusive of interannual variability) is required to produce reconstructed oscillations in lake elevation.

4. Results

4.1. Steady State Results

We found that the following precipitation multipliers produced steady state lake elevations (hereafter SSLEs) for the MCA: For *S1*, $\Delta P = 0.625$, for the *MP*, $\Delta P = 0.88$, and for *S2*, $\Delta P = 0.725$. The MCA lake level targets are shown as dashed lines in Figure 2a (*S1* in gold, *S2* in brown, and *MP* in dark blue). The current drought precipitation multiplier was calculated as $\Delta P = 0.61$. Estimated SSLEs for simulations 1, 3, 4, and 5 (see section 3)

are shown as thin lines in Figure 2a. The *S2* simulation with annual temperatures warmed by 2°C (*S2 + 2°C*) resulted in a SSLE of 1210 m (thin brown line), 11 m below the targeted S2 lowstand. The SSLE of the *Current P only* simulation was 1198 m (thin green line), which is 5 m below the targeted S1 lowstand. Including current temperature departures (annual temperature departures of +1.7°C compared to the baseline) in the *Current* simulation resulted in an SSLE of 1190 m (thin purple line), which is 13 m below the targeted S1 lowstand.

Simulated WWR streamflow for the steady state simulations is shown in Figure 2b. The *baseline* simulation (black line) produces snowmelt-driven streamflow that begins in March and peaks in May at 0.078 km^3 with a secondary peak in June at 0.076 km^3. The Stine drought simulations also peak in June at 0.036 km^3 (*S1*; dashed gold line) and 0.047 km^3 (*S2*; dashed brown line) with slightly smaller May peaks of 0.032 km^3 (S1) and 0.044 km^3 (*S2*). The *Current P only* (green line) simulation produced peak streamflow of 0.35 km^3. Both simulations where annual increases in temperatures were applied (*S2 + 2°C*; brown line and *Current*; purple line) demonstrate a 1 month shift toward earlier peak flows. Compared to the simulations where only precipitation was changed (*S2* and *Current P only*), the warmer simulations (*S2 + 2°C* and *Current*) displayed total runoff magnitudes that were reduced by 0.035 km^3 (*S2 + 2°C*) and 0.022 km^3 (*Current*) during the warm season (June–September). The *Current* climate produces 34% of the annual total runoff when compared to the *baseline* simulation (0.091 km^3 versus 0.27 km^3).

4.2. Transient MCA Lake Simulation Results

Transient lake simulation results for the MCA are also shown in Figure 2a (but as thick lines). In all cases, Walker Lake rises rapidly from the S1 lowstand (dotted gold line) during the 50 year MP interval. The MP highstand (1245 m; dotted dark blue line) is only achieved by the *baseline* climate ($\Delta P = 1$) after 38 simulation years. The estimated *MP* climate (light blue line) resulted in a final elevation of 1237 m during the MP interval. The *TCP* ($\Delta P = 1.05$) achieves a highstand of 1233 m during its 13 year duration. From the model-estimated MP highstands, the transition to the *S2* climate resulted in lake elevation falls that approached the S2 lake level (1221 m) after requiring as few as 60 years (*S2 + 2°C*; brown line) to nearly the full 200 year period (e.g., *baseline* and *MP*). The *TCP* approached the S2 lowstand after approximately 70 years. All simulations satisfied the required lake elevation fall to at least 1224 m during the S2 interval. The results for the historical *transient* simulation are shown in Figure 2c. Despite interannual variability, the simulated lake level oscillates about a mean elevation of 1255 m.

4.3. Watershed Results

Spatial watershed results are summarized in Figure 3. We assess the results in terms of the runoff ratio, which is defined as the ratio of runoff depth to precipitation depth. It is calculated annually for each model unit by summing over runoff and precipitation depths. The spatial distribution of the *baseline* simulated runoff ratios demonstrates a gradient of high runoff production (runoff ratio > 0.5) that is maximized along the Sierra Nevada crest and decreases normal to the crest in a northeasterly direction (Figure 3a). Broad areas of moderately productive ($0.2 <$ runoff ratio < 0.5) and weakly productive ($0.0 <$ runoff ratio < 0.2) runoff ratios are found along the eastern slopes of the Sierra Nevada. Approximately 80% of the watershed does not produce runoff. The difference in simulated runoff ratios of the *S1* compared to the *baseline* (Figure 3b) exhibits the largest decreases along the mountain front (0.2–0.3). Runoff ratios along the Sierra Nevada crest decrease between 0.05 and 0.1 (Figure 3b). The *Current* simulation (Figure 3c) shows similar spatial distributions of runoff ratio decreases as the *S1* simulation. However, additional decreases (0.05–0.1) are observed along the mountain front and near the Sierra Nevada crest.

Histograms of runoff ratios for the *baseline*, *S1*, and *Current* simulations are shown in Figures 3d–3f. The baseline shows the greatest number of model units contributing runoff in the moderately productive range with a secondary peak in the weakly productive range (Figure 3d). These model units are concentrated along the mountain front (Figure 3a). A tertiary peak of highly productive values shown in Figure 3d represents the Sierra Nevada crest (Figure 3a). Compared to the *baseline*, the *S1* and *Current* simulations exhibit distinct overall shifts toward smaller runoff ratio values (Figures 3e and 3f). This means that the watershed is generating less total runoff, as confirmed by reduced streamflow in these simulations (Figure 2b). Compared to the baseline, a 47% reduction in the number of model units contributing runoff is observed in the *S1* simulation while a 51% reduction is observed in the *Current* simulation. The changes captured in the histograms

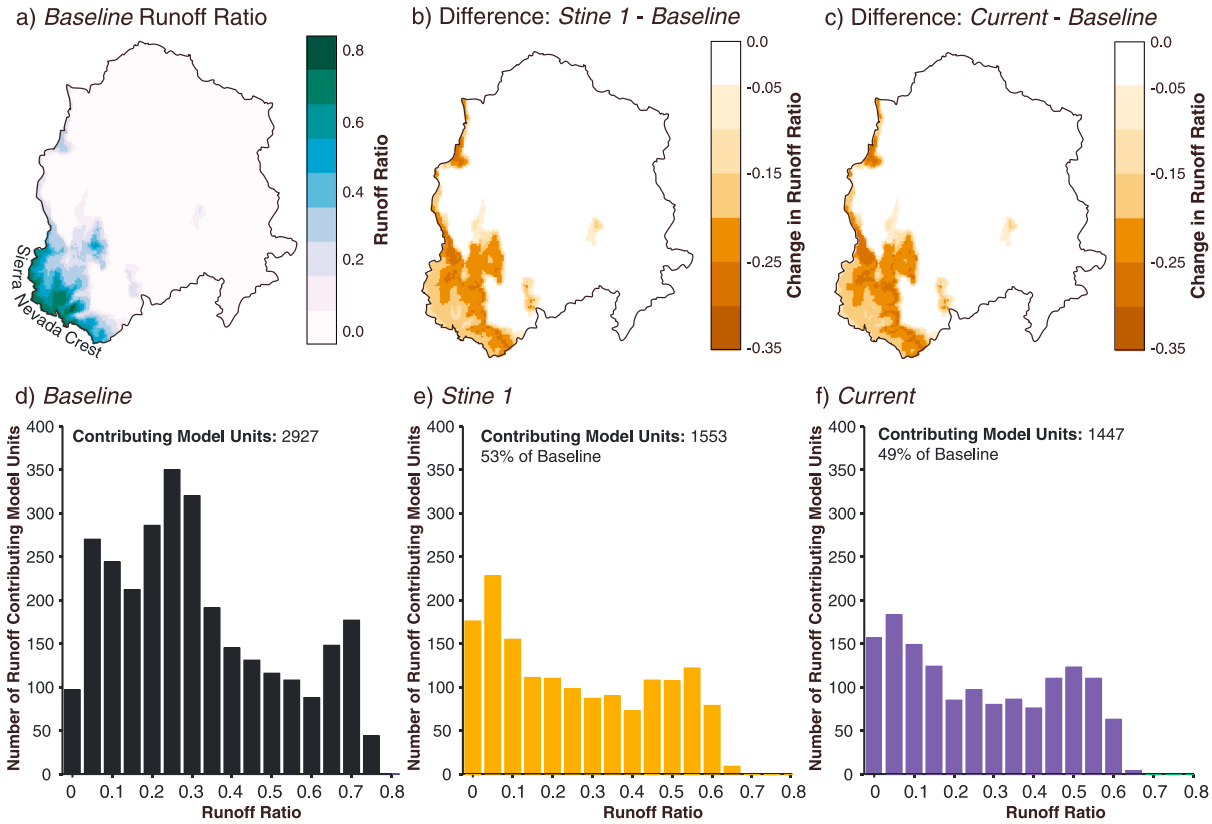

Figure 3. (a) Spatial distribution of *baseline* runoff ratios. (b and c) Simulated runoff ratio differences between the *baseline* and *S1* simulations (Figure 3b) and between the *baseline* and *Current* simulations (Figure 3c). (d–f) Histograms of runoff ratios for the *baseline* (Figure 3d), S1 (Figure 3e), and *Current* (Figure 3f) simulations.

(Figures 3e and 3f) are consistent with the greatest reductions in runoff ratios being focused along the mountain front (Figures 3b and 3c).

5. Discussion

Our results demonstrate that persistent climate regimes exert a dominant influence on the surface elevation of Walker Lake. The watershed-lake system is sensitive to changes in these regimes. Discrete transitions to relatively wetter climates produce rises in lake elevation that occur between 5 and 15 times faster than lake-level drops that result from discrete transitions to drier climates (Figure 2a). The precipitation multipliers estimated for the Stine droughts ($\Delta P = 0.62–0.725$) are on the order of those estimated during the MCA for the region ($\Delta P = 0.6–0.7$) using WBMs by *Graham and Hughes* [2007] and *Kleppe et al.* [2011]. Under continued climate conditions with near-baseline precipitation multipliers ($\Delta P = 0.88–1.05$; baseline, TCP, and MP), simulated increases in the Walker Lake level from the S1 lowstand to Holocene highstands [*Adams*, 2007] may occur within 13–50 years. These rises occur within the time constraints established from the WWR tree kill dates. Drought climates derived from steady state solutions capable of producing reconstructed high and low lake levels require 60–200 years to lower the lake from relative Holocene highstands. A rapid rise in the lake from the S1 lowstand during the MP is therefore feasible under all estimated climate conditions within the constraints given by the two sets of submerged trees. Because interannual precipitation variability alone is insufficient to drive the lake from relative highstand levels to drought levels (Figures 2c and S2), these results imply two important concepts. First, the lake acts as a low-frequency climate filter. Second, that wet or dry climate conditions must persist for multiple decades to drive large fluctuations in lake level.

The combined effects of reduced precipitation and runoff along the Sierra Nevada crest and the contraction of the contributing area along the mountain front provide the physical mechanism for the observation that the simulated lake rises much faster than it falls. As the climate becomes drier, for example, a transition from the *baseline* climate to a drought climate such as the *Current* (or *MP* to *S2*), large fractions (40–50%) of the

watershed that once contributed runoff no longer do so (Figures 3b and 3c). Further, the reduction of runoff is also due to lower runoff ratios from the contributing area of the watershed. The net effect is less inflow to the lake meaning a smaller (lower elevation) lake can be sustained against evaporative demand. However, the large volume of runoff generated in the Sierra Nevada suggests that reductions in precipitation (with temperature held constant) on the order of the Stine droughts (~35%) still produce sufficient runoff to somewhat offset evaporative demands and cause the lake level to fall slowly. In the transition to a wetter climate, i.e., the termination of S1 and onset of the MP, the opposite occurs. Increases in the fraction of watershed area contributing runoff and increased runoff productivity (higher runoff ratios) make it possible to sustain a larger (higher) lake and produce rapid rises in the lake surface area and elevation from drought lowstands (Figure 2a). The expansions and contractions of watershed contributing area occur primarily along the mountain front (Figures 3b and 3c) where large fractions of moderately to weakly productive watershed area are located and the nonlinear dependence of runoff on precipitation has the steepest gradient (Figures 3a and 3e).

The finding that the SSLE of the *S2 + 2°C* simulation is 11 m below the interpreted lowstand of the S2 period (1221 m) suggests that if the MCA were appreciably warmer than the *baseline* climate, the actual precipitation multiplier would need to be 0.77. This is larger than the estimated value of $\Delta P = 0.725$ and disagrees with other estimates of precipitation for the region [*Graham and Hughes,* 2007; *Kleppe et al.,* 2011]. Increased precipitation, either climatologically or realized through infrequent wet years, might produce streamflows in the WWR that would drown the trees. Thus, this scenario seems unlikely and demonstrates the utility of model-proxy comparisons to constrain past climates. Detailed hydraulic modeling of the WWR will be necessary to better constrain the streamflow values that would have allowed the trees to remain alive during the S1 and S2 droughts. Such modeling would also help provide constraints on the interannual variability of precipitation that produces sufficient increases in WWR streamflow to inundate the trees for longer than several weeks.

The precipitation reductions of the current drought are severe in the context of the last millennium but do not appear outside of the range of natural variability. The *Current P only* and the *S1* precipitation multipliers, simulated streamflow, and SSLEs suggest that the current drought is comparable to the more severe of the MCA droughts (Figures 2a and 2b). This is consistent with the findings of *Griffin and Anchukaitis* [2014] who showed that the current drought has large, but not unprecedented, precipitation deficits and that the observed positive temperature anomalies are contributing to the severity of the current drought [*Shukla et al.,* 2015; *Williams et al.,* 2015]. By relaxing our temperature constraints, we show how temperature increases compound the effects of reduced precipitation by increasing evaporative demand. In the warmer simulations (*S2 + 2°C* and *Current*), SSLEs are 8–11 m lower than when temperature is held constant (Figure 2a) and the shape of the hydrograph steepens and narrows (Figure 2b). These results support the concept that a warmer climate has exacerbated the current drought [*Shukla et al.,* 2015; *Williams et al.,* 2015].

The observed record high-temperature anomalies of the current drought appear outside of the range of natural variability that spans at least the past 1400 years [*Ahmed et al.,* 2013]. Anthropogenic warming has possibly contributed to the anomalous persistent high pressure responsible for the record high temperatures and current drought conditions over California and Nevada [*Wang et al.,* 2014; *Swain et al.,* 2014] although climate projections do not suggest an increase in the frequency of very dry years until the latter 21st century [*Berg and Hall*, 2015]. Nonetheless, the importance of positive temperature anomalies in increasing the severity of the current drought, as pointed out by *Griffin and Anchukaitis* [2014], *Seager et al.* [2015], *Shukla et al.* [2015], and *Williams et al.* [2015] and demonstrated in our study, suggests that the current drought exceeds the mean severity of the MCA Stine droughts. However, whether the current drought's severity is outside range of natural variability due to the anthropogenic contributions to regional warming will require additional investigations to demonstrate that its severity exceeds the most severe 4 year droughts evident in the paleoclimate records.

6. Conclusions

We employed a coupled water balance and lake evaporation model to simulate the magnitude of climate changes required to generate the prolonged medieval western U.S. droughts identified in the paleoclimate record. We examined response times of the watershed-lake system to persistent changes in climate. We also

examined the current drought and compared results to the medieval drought simulations. Our results indicate that the Stine droughts of the MCA are characterized by precipitation reductions ranging between 28 and 38% compared to the baseline climate. The current drought's average precipitation reductions in the WLB are 39%. The reductions in simulated streamflow during the current drought are consistent with simulated reductions for the Stine droughts when only precipitation is considered. Including observed temperature anomalies during the current drought demonstrates how increased evaporative demand results in a lower SSLE and provides evidence that the magnitude of the current drought is more severe than the average estimated MCA drought conditions. Our simulations were able to match the MCA lake oscillation. We demonstrated how lake rises on the order of those estimated by *Adams* [2007] could occur within 50 years under climates similar to the baseline. However, we showed that lake falls required drought conditions to persist for 60–200 years, which is broadly consistent with the documented 140–240 year long tree growth periods in the WWR.

The Stine droughts provide evidence that extended drought episodes with precipitation anomalies on the order of those being experienced today are within the range of natural climate variability. Further refinement of the geologic record will help to improve our understanding of medieval hydrology and hydroclimate, but the record is sufficient to support this conclusion from precipitation and duration perspectives. When observed temperature anomalies are included, the mean severity of the current drought exceeds the average severity of past extended droughts. A warmer and possibly drier future characterized by increased drought risks [*Cook et al.,* 2015; *Diffenbaugh et al.,* 2015] will have severe negative impacts on socioeconomic and ecological resources in the western United States. Our findings should provide additional incentive for fundamental alterations to water resource management policies in the western United States in order to improve drought resiliency under continued population growth and climatic change.

Acknowledgments

B.J.H., D.P.B., and S.D.B. received support from the National Fish and Wildlife Foundation and the Nevada State Climate Office. B.J.H. was supported by a NASA Nevada Space Grant Graduate Fellowship under award NNX10AN23H. A.E.P. was supported by the Lamont-Doherty Earth Observatory, the Gary Comer Science and Education Foundation, and the Lenfest Foundation. We thank Chris Garner for helpful discussions. Park Williams and an anonymous reviewer provided thoughtful comments that greatly improved this work. All data for this paper are properly cited and referred to in the reference list; model output is available upon request (benjamin.hatchett@gmail.com). This is LDEO contribution 7936.

The Editor thanks two anonymous reviewers for their assistance in evaluating this paper.

References

Adams, K. D. (2007), Late Holocene lake-level fluctuations and sedimentary environments at Walker Lake, Nevada, USA, *Geol. Soc. Am. Bull.*, *119*, 126–139.

Ahmed, M., et al. (2013), Continental-scale temperature variability during the past two millennia, *Nat. Geosci.*, *6*, 339–346, doi:10.1038/ngeo1797.

Benson, L., M. Kashgarian, R. O. Rye, S. P. Lund, F. L. Paillet, J. Smoot, C. Kester, S. Mensing, D. Meko, and S. Lindstrom (2002), Holocene multidecadal and multicentennial droughts affecting Northern California and Nevada, *Quat. Sci. Rev.*, *21*, 659–682.

Berg, N., and A. Hall (2015), Increased interannual precipitation extremes over California under climate change, *J. Clim.*, *28*, 6324–6334, doi:10.1175/JCLI-D-14-00624.1.

Borsa, A. A., D. C. Agnew, and D. R. Cayan (2014), Ongoing drought-induced uplift in the western United States, *Science*, *345*(6204), 1587–1590.

Broecker, W. S. (2010), Long-term water prospects in the western United States, *J. Clim.*, *23*, 6669–6683.

Broecker, W. S., and A. E. Putnam (2013), Hydrologic impacts of past shifts of Earth's thermal equator offer insight into those to be produced by fossil fuel CO_2, *Proc. Natl. Acad. Sci. U.S.A.*, *110*, 16,710–16,715.

California Department of Water Resources (2015), Water Deliveries, State Water Project Analysis Office. [Available at http://www.water.ca.gov/swpao/deliveries.cfm.]

Cayan, D., T. Das, D. Pierce, T. Barnett, M. Tyree, and A. Gershunov (2010), Future dryness in the southwest United States and the hydrology of the early 21st century drought, *Proc. Natl. Acad. Sci. U.S.A.*, *107*(50), 21,271–21,276.

Cook, B. I., R. Seager, and R. L. Miller (2011), On the causes and dynamics of the early twentieth-century North American pluvial, *J. Clim.*, *24*, 5043–5060, doi:10.1175/2011JCLI4201.1.

Cook, B. I., T. R. Ault, and J. E. Smerdon (2015), Unprecedented 21st-century drought risk in the American Southwest and Central Plains, *Sci. Adv.*, *1*, e1400082, doi:10.1126/sciadv.1400082.

Cook, E. R., and P. Krusic (2004), North American summer PDSI reconstructions, Data Contribution Series No. 2004-045, IGBP PAGES/World Data Center for Paleoclimatology, NOAA/NGDC Paleoclimatology Program, Boulder, Colo.

Cook, E. R., C. A. Woodhouse, C. M. Eakin, D. M. Meko, and D. W. Stahle (2004), Long-term aridity changes in the western United States, *Science*, *306*, 1015–1018, doi:10.1126/science.1102586.

Cook, E. R., R. R. Heim, C. Herweijer, and C. Woodhouse (2010), Megadroughts in North America: Placing IPCC projections of hydroclimatic change in a long-term paleoclimate context, *J. Quat. Sci.*, *25*, 48–61, doi:10.1002/jqs.1303.

Dai, A. (2013), Increasing drought under global warming in observations and models, *Nat. Clim. Change*, *3*(1), 52–58.

Dai, A., K. E. Trenberth, and T. Qian (2004), A global dataset of Palmer Drought Severity Index for 1870–2002: Relationship with soil moisture and effects of surface warming, *J. Hydrometeorol.*, *5*(6), 1117–1130.

Daly, C., R. P. Neilson, and D. L. Phillips (1994), A statistical-topographic model for mapping climatological precipitation over mountainous terrain, *J. Appl. Meteorol.*, *33*, 140–158, doi:10.1175/1520-0450(1994)033<0140:ASTMFM>2.0.CO;2.

Diffenbaugh, N. S., D. L. Swain, and D. Touma (2015), Anthropogenic warming has increased drought risk in California, *Proc. Natl. Acad. Sci. U.S.A.*, *112*(13), 3931–3936, doi:10.1073/pnas.1422385112.

Graham, N. E., and M. K. Hughes (2007), Reconstructing the Medieval low stands of Mono Lake, Sierra Nevada, California, USA, *Holocene*, *17*, 1197–1210.

Gray, S. T., and G. J. McCabe (2010), A combined water balance and tree ring approach to understanding the potential hydrologic effects of climate change in the central Rocky Mountain region, *Water Resour. Res.*, *46*, W05513, doi:10.1029/2008WR007650.

Griffin, D., and K. J. Anchukaitis (2014), How unusual is the 2012–2014 California drought?, *Geophys. Res. Lett.*, *41*, 9017–9023, doi:10.1002/2014GL062433.

Howitt, R., J. Medellin-Azuara, D. MacEwan, J. Lund, and D. Sumner (2014), Economic analysis of the 2014 drought for California Agriculture, 20 pp., Cent. for Watershed Sci., Univ. of Calif., Davis. [Available at https://watershed.ucdavis.edu/files/biblio/DroughtReport_23July2014_0.pdf.]

Kleppe, J. A., D. S. Brothers, G. M. Kent, F. Biondi, S. Jensen, and N. W. Driscoll (2011), Duration and severity of Medieval drought in the Lake Tahoe Basin, *Quat. Sci. Rev.*, *30*, 3269–3279.

Malamud-Roam, F., and B. L. Ingram (2004), Late Holocene $\delta^{13}C$ and pollen records of paleosalinity from marshes in the San Francisco Bay estuary, California, *Quat. Res.*, *62*, 134–145.

Mann, M. E., Z. Zhang, S. Rutherford, R. S. Bradley, M. K. Hughes, D. Shindell, C. Ammann, G. Faluvegi, and F. Ni (2009), Global signatures and dynamical origins of the Little Ice Age and Medieval Climate Anomaly, *Science*, *326*, 1256–1260, doi:10.1126/science.1177303.

McCabe, G. J., and S. L. Markstrom (2007), A monthly water balance model driven by a graphical user interface, *U.S. Geol. Surv. Open File Rep., 2007-1088*, 12 pp.

McCabe, G. J., and D. M. Wolock (2007), Warming may create substantial water supply shortages in the Colorado River basin, *Geophys. Res. Lett.*, *34*, L22708, doi:10.1029/2007GL031764.

McCabe, G. J., and D. M. Wolock (2014), Variability common to global sea surface temperatures and runoff in the conterminous United States, *J. Hydrometeorol.*, *15*, 714–725, doi:10.1175/JHM-D-13-097.1.

Mearns, L. O., et al. (2012), The North American regional climate change assessment program overview of phase I results, *Bull. Am. Meteorol. Soc.*, *93*, 1337–1362, doi:10.1175/BAMS-D-11-00223.2.

Montenegro, S., and R. Ragab (2012), Impact of possible climate and land use changes in the semi arid regions: A case study from North Eastern Brazil, *J. Hydrol.*, *434–435*, 55–86, doi:10.1016/j.jhydrol.2012.02.036.

Priestley, C. H. B., and R. J. Taylor (1972), On the assessment of a surface heat flux and evaporation using large-scale parameters, *Mon. Weather Rev.*, *100*, 81–92, doi:10.1175/1520-0493(1972)100<0081:OTAOSH>2.3.CO;2.

Saito, L., F. Biondi, R. Devkota, J. Vittori, and J. D. Salas (2014), A water balance approach for reconstructing streamflow using tree-ring proxy records, *J. Hydrol.*, doi:10.1016/j.jhydrol.2014.11.022, in press.

Schladow, G. (2014), Tahoe: State of the lake report 2014, 91 pp., Tahoe Environ. Res. Cent., Univ. of Calif., Davis. [Available at http://terc.ucdavis.edu/stateofthelake/sotl-reports/2014/sotl_2014_complete.pdf].

Seager, R., et al. (2007), Model projections of an imminent transition to a more arid climate in Southwestern North America, *Science*, *316*, 1181–1184, doi:10.1126/science.1139601.

Seager, R., M. Hoerling, S. Schubert, H. Wang, B. Lyon, A. Kumar, J. Nakamura, and N. Henderson (2015), Causes of the 2011 to 2014 California drought, *J. Clim.*, doi:10.1175/JCLI-D-14-00860.1, in press.

Shukla, S., M. Safeeq, A. AghaKouchak, K. Guan, and C. Funk (2015), Temperature impacts on the water year 2014 drought in California, *Geophys. Res. Lett.*, *42*, 4384–4393, doi:10.1002/2015GL063666.

Stakhiv, E. Z. (2011), Pragmatic approaches for water management under climate change uncertainty, *J. Am. Water Resour. Assoc.*, *47*(6), 1183–1196, doi:10.1111/j.1752-1688.2011.00589.x.

Stine, S. (1990), Late Holocene fluctuations of Mono Lake, eastern California, *Palaeogeogr. Palaeoclimatol. Palaeoecol.*, *78*, 333–381.

Stine, S. (1994), Extreme and persistent drought in California and Patagonia during mediaeval time, *Nature*, *369*, 546–549.

Swain, D., M. Tsiang, M. Haughen, D. Singh, A. Charland, B. Rajarthan, and N. Diffenbaugh (2014), The extraordinary California drought of 2013/2014: Character, context and the role of climate change, in *Explaining Extreme Events of 2013 From a Climate Perspective*, *Bull. Am. Meteorol. Soc.*, edited by S. C. Herring et al., pp. S3–S6, Am. Meteorol. Soc., Boston, Mass., doi:10.1175/1520-0477-95.9.S1.1.

U.S. Bureau of Reclamation (2015), Central Valley Project Water Quantities with 2015 Allocation. [Available at http://www.usbr.gov/mp/PA/water/docs/1_CVP_Water_Quantities_Allocation.pdf.]

Wang, H., and S. Schubert (2014), Causes of the extreme dry conditions over California during early 2013, *Bull. Am. Meteorol. Soc.*, *95*(9), S7–S11.

Wang, S., L. Hipps, R. R. Gillies, and J. Yoon (2014), Probable causes of the abnormal ridge accompanying the 2013–2014 California drought: ENSO precursor and anthropogenic warming footprint, *Geophys. Res. Lett.*, *41*, 3220–3226, doi:10.1002/2014GL059748.

Williams, A. P., R. Seager, J. T. Abatzoglou, B. I. Cook, J. E. Smerdon, and E. R. Cook (2015), Contribution of anthropogenic warming to California drought during 2012–2014, *Geophys. Res. Lett.*, *42*, 6819–6828, doi:10.1002/2015GL064924.

Woodhouse, C. A., K. E. Kunkel, D. R. Easterling, and E. R. Cook (2005), The twentieth-century pluvial in the western United States, *Geophys. Res. Lett.*, *32*, L07701, doi:10.1029/2005GL022413.